
Conformal Prediction Adaptive to Unknown Subpopulation Shifts

Nien-Shao Wang
 University of Southern California
`nienwang@usc.edu`

Duygu Nur Yaldiz
 University of Southern California
`yaldiz@usc.edu`

Yavuz Faruk Bakman
 University of Southern California
`ybakman@usc.edu`

Sai Praneeth Karimireddy
 University of Southern California
`karimire@usc.edu`

Abstract

Conformal prediction is widely used to equip black-box machine learning models with uncertainty quantification enjoying formal coverage guarantees. However, these guarantees typically break down in the presence of distribution shifts, where the data distribution at test time differs from the training (or calibration-time) distribution. In this work, we address subpopulation shifts, where the test environment exhibits an unknown and differing mixture of subpopulations compared to the calibration data. We propose new methods that provably adapt conformal prediction to such shifts, ensuring valid coverage without requiring explicit knowledge of subpopulation structure. Our algorithms scale to high-dimensional settings and perform effectively in realistic machine learning tasks. Extensive experiments on vision (with vision transformers) and language (with large language models) benchmarks demonstrate that our methods reliably maintain coverage and controls risk in scenarios where standard conformal prediction fails.

1 Introduction

In high-stakes real-world applications of machine learning, such as healthcare, uncertainty quantification (UQ) is crucial to safeguard patient health from the risks posed by model uncertainty. Conformal prediction techniques [32] offer a framework for uncertainty quantification before model deployment. Conformal prediction operates similarly to a doctor’s differential diagnosis. A doctor gathers patient data and uses medical expertise to eliminate unlikely conditions, narrowing down to a list of probable diagnoses. Similarly, conformal prediction produces a set of possible labels, with a high probability that the true label lies within this set. The size of the prediction set reflects the model’s uncertainty—the larger the set, the greater the uncertainty, and vice versa.

Formally, conformal prediction guarantees marginal coverage, meaning that for a given input X_{test} with unknown label Y_{test} and a user-defined error rate α , the probability that Y_{test} lies in the prediction set $C_\alpha(X_{\text{test}})$ is at least $1 - \alpha$, i.e.,

$$\Pr(Y_{\text{test}} \in C_\alpha(X_{\text{test}})) \geq 1 - \alpha. \quad (1)$$

The size of the prediction set $C_\alpha(X_{\text{test}})$ reflects the level of uncertainty—larger sets indicate higher uncertainty, while smaller sets signal greater confidence. The threshold used in conformal prediction determines how conservative the prediction set is, balancing between marginal coverage and uncertainty.

Standard conformal prediction offers provable marginal coverage guarantees under the assumption that test data is exchangeable with the training data. However, in many real-world scenarios, this

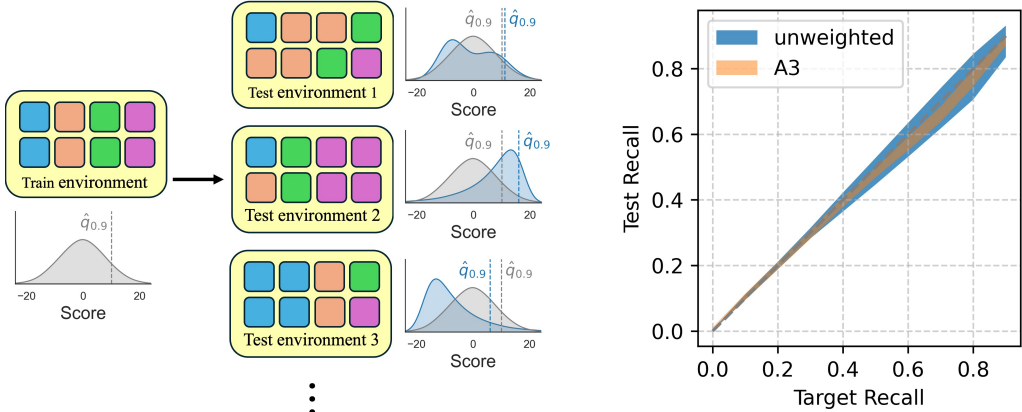


Figure 1: (Left) Example of subpopulation shifts with 4 domains. Each colored square represents data from a particular domain. Train and test environments are mixtures of the same set of domains but at different proportion. Score distributions (gray for train environment and blue for each test environment) and threshold calculated from standard conformal prediction are shown for each train/test environment. Subpopulation shift for test environment 1 leads to roughly the ideal coverage while shifts for test environment 2 and 3 lead to significant under and over-coverage respectively. (Right) The same issue arises in LLM hallucination detection across different test environments. Standard LLM uncertainty estimation method (blue) is sensitive to distribution shifts displaying high variance in its hallucination detection recall across test-environments, while the recall with our modification (orange) tightly follows the desired target recall.

assumption is violated due to distribution shifts. One of the most common types of distribution shift is subpopulation shift, where the proportions of subpopulations differ between training and deployment environments [34]. A key challenge arises when different subpopulations present varying levels of prediction difficulty, requiring distinct thresholds to maintain reliable marginal coverage across all subpopulations. Distribution shifts, particularly subpopulation shifts, complicate this task further by causing the proportions of subpopulations to differ between training and test environments. As a result, a uniform threshold might not provide adequate marginal coverage for all subpopulations.

To address this, we propose a two-stage approach. First, we train a domain classifier that, given a test input X , predict a probability distribution over the subpopulations X belong to. We then use the predicted probabilities to weigh the calibration data to adapt the threshold for conformal prediction accordingly, ensuring the prediction set reflects the uncertainty appropriate for each subpopulation.

Key contributions. We make three contributions to the problem of adapting conformal prediction to unknown subpopulation shift settings.

- We introduce a novel class of algorithms that are adaptive to arbitrary mixtures over domains by utilizing a learnt *domain classifier*. These can be seen as *test-time adaptation* methods that adaptively adjust the conformal prediction threshold. We prove that under mild assumptions, our new algorithms guarantee tight coverage for arbitrary subpopulation shifts.
- We extend to the setting when we have no knowledge of the domains (either at calibration time or test time). In this case, we adaptively filter and reweight the calibration data to adaptively pick a threshold for each test data point.
- We run extensive experiments simulating realistic subpopulation shifts on high-dimensional vision classification datasets. We show that our methods consistently provide tight coverage across test environments, whereas standard conformal prediction under or over-covers.
- We also extend our methods to the conformal risk control where we are tasked with controlling the *hallucination risk* in large language models (LLMs). We show that our methods improve upon the state of the art uncertainty estimation for short-form question answering tasks and provide tighter recall under distribution shifts.

2 Problem Setup

2.1 Background

Notation. We let \mathcal{X} and \mathcal{Y} denote the input and target space of a multiclass classification task. $\hat{f} : \mathcal{X} \rightarrow \Delta^J$ is the pre-trained classifier for the classification task and the output of \hat{f} is a probability distribution over J possible outcomes, e.g., the softmax output of a neural network. $\hat{f}(X)_i$ represents the i -th entry of the output of \hat{f} . We let $z : \mathcal{X} \rightarrow \mathbb{R}^d$ denote an embedding function that maps the input into a d -dimensional embedding space, and $h : \mathbb{R}^d \times \mathbb{R}^d \rightarrow \mathbb{R}$ stands for some similarity function between embeddings.

We denote by \mathbb{P}_k the distribution of the k -th domain, where there are K domains in total. The calibration dataset from the k -th domain is represented as $\{(X_i^k, Y_i^k); \hat{f}\}_{i=1}^{n_k}$, and each pair (X_i^k, Y_i^k) is assumed to be drawn i.i.d. from \mathbb{P}_k . The overall calibration dataset is sampled from the training environment $\mathbb{P}_{\text{train}}$, which is a mixture of the K domain distributions. The score function is represented by $S : \mathcal{X} \times \mathcal{Y} \rightarrow \mathbb{R}$ and will make use of \hat{f} . We define $m_k(q)$ as $|\{S(X_i^k, Y_i^k; \hat{f}) \leq q\}|$, which is the number of calibration data in domain k with score less than or equal to q .

Lastly, the test set is denoted by $\{(X_{\text{test}}^i, Y_{\text{test}}^i)\}_{i=1}^{n_{\text{test}}}$. These samples are drawn from a test environment \mathbb{P}_{test} , which is an unknown mixture of domains. We denote the set of all possible test environments by \mathcal{D} . Examples of such test environments are illustrated in Figure 1.

Score Functions A score function maps an input pair (X, Y) to a real-valued score. A larger score indicates less conformity between (X, Y) and other training data. Conformal Prediction allows an arbitrarily defined score function, however, it could give uninformative prediction sets. For the vision task, we examine our methods with 3 score functions: Least Ambiguous Set-valued Classifier (LAC) [28], Adaptive Prediction Set (APS) [26], and Regularized Adaptive Prediction Set (RAPS) [2]. For the language task, we examine 3 score functions: Length Normalized Scoring (LNS) [21], Meaning-Aware Response Scoring (MARS) [5], and Degree Matrix Uncertainty [19].

Conformal Prediction Under Exchangeability Given a test data X_{test} with unknown label Y_{test} , a calibration set $\{(X_i, Y_i)\}_{i=1}^n$, which is distinct from train and test set, and a user defined error rate α , the goal of conformal prediction is to build a prediction set C_α that satisfies 1. To conformalize a model to output a valid prediction set, the following procedure is followed: First, a score function S is defined. Second, the threshold \hat{q}_α is computed as the $\frac{\lceil(n+1)(1-\alpha)\rceil}{n}$ quantile of $\{S(X_i, Y_i; \hat{f})\}_{i=1}^n$. Lastly, the prediction set $C_\alpha(X_{\text{test}})$ is returned such that $C_\alpha(X_{\text{test}}) = \{y | S(X_{\text{test}}, y; \hat{f}) \leq \hat{q}_\alpha\}$. If the calibration data and the test data are drawn i.i.d from the same domain, then $C(X_{\text{test}})$ satisfies the marginal coverage guarantee due to exchangeability between calibration and test data [3]. We refer to this method as the standard or unweighted conformal prediction throughout the paper.

Conformal Risk Control The conformal prediction framework can be extended to provide guarantee beyond coverage. Given a prediction set $C_{\hat{\lambda}}(X_{\text{test}}) = \{y | S(X_{\text{test}}, y) \leq \hat{\lambda}\}$, a loss function ℓ that decreases as $|C_{\hat{\lambda}}(X_{\text{test}})|$ increases, and a user defined error rate α , the conformal risk control guarantee is defined as,

$$\mathbb{E}[\ell(C_{\hat{\lambda}}(X_{\text{test}}), Y_{\text{test}})] \leq \alpha \quad (2)$$

[4]. Note that the marginal coverage guarantee can be reduced to 2 if we define ℓ as the miscoverage loss, i.e., $\ell(C_{\hat{\lambda}}(X_{\text{test}}), Y_{\text{test}}) = \mathbb{1}\{Y_{\text{test}} \notin C_{\hat{\lambda}}(X_{\text{test}})\}$. We refer to [4] for the details of conformal risk control. One application for the conformal risk control framework is in large language model (LLM) uncertainty estimation, in particular, hallucination detection. Hallucination refers to when an LLM generate responses that are factually false or inconsistent with the training data. Conformal risk control can be used to select a threshold to determine whether an LLM output is a hallucination or not while maintaining a theoretical bound to metrics such as sensitivity or precision.

2.2 Conformal Prediction under Subpopulation Shifts

Subpopulation Shifts. The standard conformal prediction procedure relies on the exchangeability assumption between calibration and test data. However, in many real-world scenarios—such as dynamic time series—this assumption often does not hold [23]. In this work, we focus on the setting

of subpopulation shifts. Specifically, the calibration data is drawn from one of the K in-domain distributions, denoted by \mathbb{P}_k . In contrast, the test data is sampled i.i.d. from a test environment \mathbb{P}_{test} , which is a mixture of these in-domain distributions, i.e.,

$$\mathbb{P}_{\text{test}} = \sum_{k=1}^K \lambda_k \mathbb{P}_k, \quad (3)$$

where λ_k is the probability that \mathbb{P}_{test} is drawn from \mathbb{P}_k . During test time, λ_k 's are unknown.

Failure of Standard Conformal Prediction. Under standard conformal prediction, the marginal coverage in Equation 1 is not guaranteed if the test data is not exchangeable with the calibration data due to subpopulation shifts. For instance, if the test environment has higher probability to be drawn from a harder domain, i.e., λ_k is large for domain k where data typically receive higher scores, then standard conformal prediction would result in under-coverage. Conversely, if λ_k is large for domain k which has data with lower scores, it would lead to over-coverage. As illustrated in Figure 1, test environment 2 exhibits under-coverage, while test environment 3 demonstrates over-coverage.

Prior Approaches To tackle the issue caused by distribution shifts, we need to weigh calibration data from each domain accordingly based on the test environment. [31] proposes a weighted version of conformal prediction for the case of generic covariate shifts, i.e., the input of the calibration data X is drawn from some distribution \mathcal{P} while the input of the test data X_{n+1} is drawn from some distribution $\tilde{\mathcal{P}}$. The method weighs the score of each calibration data by its likelihood ratio, $d\tilde{\mathcal{P}}/d\mathcal{P}$ and is able to achieve 1. However, the method requires either (1) knowledge of $\tilde{\mathcal{P}}$ and \mathcal{P} at test time or (2) an extra held out set drawn from the test environment to estimate $d\tilde{\mathcal{P}}/d\mathcal{P}$. For case 1, λ is unknown at test time so $\tilde{\mathcal{P}}$ is not known while for case 2, test data might be scarce so an estimate of the likelihood ratio is not possible. Another method to adapt conformal prediction to distribution shifts is proposed by [6]. In that work, distribution shifts that make the score large are estimated and marginal coverage guarantee is provided for such shifts. To adapt this idea to our settings, the worst case shift is the case when the test environment is drawn from the hardest domain completely, i.e., the $\mathbb{P}_{\text{test}} = \mathbb{P}_k$ where the score from domain k are typically larger than all other domains.

3 Adapting to subpopulation shifts with known domains

3.1 Weighted Conformal Prediction

To solve the issue caused by distribution shifts, we need to weigh calibration data from each domain differently based on the test environment. For example, if λ_k is high, we will need to weight calibration data from domain k higher since \mathbb{P}_k represents the test environment more closely. To find the correct weighting, we propose Algorithm 1 which takes a separate model, $c : \mathcal{X} \rightarrow [0, 1]^K$, named domain classifier, to predict the true $Pr((X_{\text{test}}, Y_{\text{test}}) \sim \mathbb{P}_k | X_{\text{test}})$ for each domain k . Theorem 3.1 states that if c is a Bayes-optimal classifier, then we get marginal coverage guarantee.

Theorem 3.1. *If c is a Bayes-optimal classifier, the output of Algorithm 1 C_α , satisfies $(1 - \alpha)$ coverage as in eqn. (1).*

The proof of Theorem 3.1 can be found in Appendix A.1. Intuitively, if we have a Bayes-optimal domain classifier, the weight given to the domains which are more likely should be higher. In fact, by weighting the calibration scores based on λ , we can adopt the partial exchangeability proof of [20] to prove our claim. In the extreme case where the test environment is one of the K in-distribution domains, i.e. $(X_{\text{test}}, Y_{\text{test}}) \sim \mathbb{P}_{\text{test}} = \mathbb{P}_k$, we have that $\hat{\lambda}(X_{\text{test}})_i = 1$ for $i = k$ and 0 otherwise. We see that the Algorithm 1 reduces to the case of standard conformal prediction which satisfies 1 since $(X_{\text{test}}, Y_{\text{test}})$ is now exchangeable with calibration data from domain k .

3.2 Conformal Prediction with multicalibrated domain classifier

In most cases, training a perfect classifier is impossible. Therefore, since c can only provide the estimated probability distribution, how well calibrated c is matters a lot to the coverage provided by Algorithm 1, especially in cases where the in-domain distributions differ a lot. Therefore, it's

Algorithm 1

Input : pre-trained model \hat{f} , domain classifier c , calibration sets $\{(X_i^k, Y_i^k)\}_{i=1}^{n_k}$ where $k \in [K]$, score function S , error rate α , test data X_{test}

Output : prediction set C_α

```

Calculate score,  $s_i^k$ , for each calibration data  $(X_i^k, Y_i^k)$ 
 $\hat{\lambda} \leftarrow c(X_{\text{test}})$ 
 $\hat{q}_\alpha \leftarrow \min_{\hat{q}} \sum_{k=1}^K \frac{\hat{\lambda}_k m_k(\hat{q}_\alpha)}{n_k + 1} \geq (1 - \alpha)$   $\triangleright \lambda_k$  is the  $k$ -th entry of the softmax output of  $c$ 
 $C_\alpha \leftarrow \{j \in J | S(X_{\text{test}}, j; \hat{f}) \leq \hat{q}_\alpha\}$ 
return  $C_\alpha$ 

```

Algorithm 2

Input : pre-trained model \hat{f} , domain classifier c , calibration sets $\{(X_i^k, Y_i^k)\}_{i=1}^{n_k}$ where $k \in [K]$, score function S , error rate α , test data set $\{X_{\text{test}}^i\}_{i=1}^{n_{\text{test}}}$

Outut : prediction set C_α

```

Calculate score,  $s_i^k$ , for each calibration data  $(X_i^k, Y_i^k)$ 
Calculate  $\hat{\lambda}$  as the mean of  $c(X_{\text{test}}^i)$  across the test data set.
 $\hat{q}_\alpha \leftarrow \min_{\hat{q}} \sum_{k=1}^K \frac{\hat{\lambda}_k m_k(\hat{q}_\alpha)}{n_k + 1} \geq (1 - \alpha)$   $\triangleright \lambda_k$  is the  $k$ -th entry of the softmax output of  $c$ 
 $C_\alpha \leftarrow \{j \in J | S(X_{\text{test}}, j; \hat{f}) \leq \hat{q}_\alpha\}$ 
return  $C_\alpha$ 

```

more feasible to train a domain classifier that makes mistakes within a limited range. We will use the notion of multicalibration, which is used to measure fairness of a predictor [14].

Definition 3.2. Denote \mathcal{G} as a family of subsets of \mathcal{X} , $\tilde{p} : \mathcal{X} \rightarrow \Delta^K$ as some predictor, and $p^* : \mathcal{X} \rightarrow \Delta^K$ as the true probability distribution. \tilde{p} is multicalibrated with respect to \mathcal{G} if for all $v \in \tilde{p}(\mathcal{X})$ and $G \in \mathcal{G}$,

$$\mathbb{E}(p^*(x)|x \in G, \tilde{p}(x) = v) = v.$$

By defining the family of subsets, \mathcal{G} , as the set of all possible test environments and assuming that the domain classifier, c , from Algorithm 1 is multicalibrated with respect to \mathcal{G} , we can ensure coverage conditioned on each test environment as shown in Theorem 3.3

Theorem 3.3. Suppose \mathcal{G} is the set of all test environments and c is multicalibrated with respect to \mathcal{G} . Then the output of Algorithm 1, C_α , satisfies

$$\Pr(Y_{\text{test}} \in C(X_{\text{test}}) | (X_{\text{test}}, Y_{\text{test}}) \sim \mathbb{P}_{\text{test}}) \geq 1 - \alpha$$

The proof of Theorem 3.3 can be found in Appendix A.2. While the results of Theorem 3.1 and 3.3 are very similar, they provide coverage guarantee under different assumptions. In Theorem 3.1, we assume that c is a Bayes-optimal classifier which allows us to know λ exactly. However, in Theorem 3.3, we made a vastly weaker but sufficient assumption that c is multicalibrated. The assumption allows the true λ to be predicted by c on average to recover a similar conditional coverage guarantee.

3.3 Conformal Prediction with multiaccurate domain classifier

While learning multicalibrated predictors is easier than learning the Bayes-optimal classifier, they are still shown to have high computational and sample complexity which makes it difficult to train [10]. Therefore, an even more relaxed assumption is necessary in most cases, which motivates us to use the notion of multiaccuracy [17].

Definition 3.4. Denote \mathcal{G} as a family of subsets of \mathcal{X} , $\tilde{p} : \mathcal{X} \rightarrow \Delta^K$ as some predictor, and $p^* : \mathcal{X} \rightarrow \Delta^K$ as the true probability distribution. \tilde{p} is multiaccurate with respect to \mathcal{G} if for all $G \in \mathcal{G}$,

$$\mathbb{E}(p^*(x)|x \in G) = \mathbb{E}(\tilde{p}(x)|x \in G).$$

Under Definition 3.4, multiaccuracy relaxes the definition of multicalibration and only requires a predictor to be calibrated within a subset of \mathcal{X} . Therefore, we propose Algorithm 2, where $\hat{\lambda}$ is the

mean of $c(X_{\text{test}}^i)$ over the test data set instead. By defining the family of subsets, \mathcal{G} , as the set of all possible test environments and assuming that c from Algorithm 2 is multiaccurate, we can ensure coverage conditioned on each test environment as shown in Theorem 3.5.

Theorem 3.5. *Suppose \mathcal{G} is the set of all test environments and c is multiaccurate with respect to \mathcal{G} . Then the output of Algorithm 2, \mathcal{C}_α , satisfies*

$$\Pr(Y_{\text{test}} \in C(X_{\text{test}}) | (X_{\text{test}}, Y_{\text{test}}) \sim \mathbb{P}_{\text{test}}) \geq 1 - \alpha$$

Comparing to Theorem 3.5 to Theorem 3.3, They provide the same coverage guarantee conditioned on $(X_{\text{test}}, Y_{\text{test}}) \sim \mathbb{P}_{\text{test}}$, however, they differ in assumptions. Theorem 3.5 uses a more relaxed assumption which leads to the change between Algorithm 1 and Algorithm 2. In some sense Algorithm 2 is easier to provide coverage guarantee for because multiaccuracy can be achieved more efficiently.

Remark 1. *As mentioned previously, multicalibration is a property that is difficult to formally prove. However, [11] conducted a comprehensive study evaluating the effectiveness of multicalibration post-processing across diverse datasets (including tabular, image, and language) and models ranging from simple decision trees to 90 million parameter fine-tuned LLMs. The study found that models which are well trained tend to be relatively multicalibrated without requiring additional post-processing. Thus, we believe that assuming access to a multi-accuracy classifier c is an easy to satisfy assumption.*

4 Adapting to subpopulation shifts without domain information

The two proposed algorithms so far both assume the knowledge of domains at both train and test time, although the exact mixture for the test environments at test time is unknown. To expand on the previous ideas, we empirically study the case where the calibration set, sampled from $\mathbb{P}_{\text{train}}$, is given but we have no knowledge of which of the K domains each calibration data belong to.

4.1 Conformal Prediction weighted by similarity measures

In many real word tasks, similarity measures in the representation space often capture the semantic similarity between images or languages. Therefore, we propose Algorithm 3 which assumes that data with higher similarities in the embedding space have higher probability to be from the same domain. Algorithm 3 is exactly the weighted conformal prediction method proposed by [31] where instead of weighing the calibration data by the likelihood ratio, we propose weighing the calibration data by similarity between the embedding of each calibration data and the test data. Weighting by similarity measures assumes that data with high similarity measures are semantically similar, i.e., from the same or similar domains. However, empirical results show that such assumption is not true across all domains, therefore, we propose keeping only a fraction of the data with the highest similarity measures to the test data. The percentage of data to include is defined as β in Algorithm 3.

4.2 Conformal risk control for LLM hallucination detection

The same framework from 4.1 can be extended to make binary decisions, e.g., LLM hallucination detection in short-form question answering tasks. To achieve this, we will use the conformal risk control to lower bound the test recall for detecting hallucination with r_{test} , where hallucinated generations are class 1. Formally, given a test data $(X_{\text{test}}, Y_{\text{test}})$, a target recall r_{test} , we wish to construct $C : \mathcal{Y} \rightarrow \{\pm 1\}$ such that

$$\mathbb{E}[\Pr(C(Y_{\text{test}}^*) = 1 | A(X_{\text{test}}, Y_{\text{test}}, Y_{\text{test}}^*) = 1)] \geq r_{\text{test}}$$

where Y_{test}^* is the greedy output to the query X_{test} , Y_{test} is the ground truth and $A(X_{\text{test}}, Y_{\text{test}}, Y_{\text{test}}^*) = 1$ if Y_{test}^* is a hallucinated response to query X_{test} and 0 otherwise. We will follow the steps from Algorithm 3 and make necessary adjustments. Specifically, first, since we wish to bound the recall error, all calibration data are hallucinated generations. Second, we compute the score using score function $S : \mathcal{X} \times \mathcal{Y} \rightarrow \mathbb{R}$, which uses a generative model \hat{f} . We note that this scoring function is different from the score functions from the vision tasks, as the score does not take the ground truth into account. We then follow the same steps in Algorithm 3 to find the threshold \hat{q}_α where we let α to be $1 - r_{\text{test}}$. Lastly, we label the test data “hallucination” if the score is above \hat{q}_α and “not hallucination” otherwise.

Algorithm 3

Input : pre-trained model \hat{f} , embedding function z , calibration sets $\{(X_i, Y_i)\}_{i=1}^n$, score function S , error rate $\alpha, \beta \in [0, 1]$, similarity function $h, \sigma \in \mathbb{R}$, test data X_{n+1}

Output : prediction set C_α

$$n' \leftarrow \lceil \beta n \rceil$$

Keep the top n' calibration data, ranked by similarity to X_{n+1} . The remaining calibration data is denoted by (X'_i, Y'_i) and the test data is denoted by $(X'_{n'+1}, Y'_{n'+1})$

Calculate score, s_i , for each calibration data (X'_i, Y'_i)

$$s_{n+1} \leftarrow \infty$$

$\gamma_i \leftarrow h(z(X'_{n'+1}), z(X'_i))$ for $i = 1, 2, \dots, n' + 1$.

$m \leftarrow \text{Softmax}(\{\gamma_i/\sigma\})$

$$\hat{q}_\alpha \leftarrow \text{Quantile} \left(1 - \alpha, \sum_{i=1}^{n'+1} m_i \delta_{s_i} \right)$$

$\triangleright \delta_{s_i}$ denotes a point mass at s_i

$$C_\alpha \leftarrow \{j \in J \mid S(X_{\text{test}}, j; \hat{f}) \leq \hat{q}_\alpha\}$$

return C_α

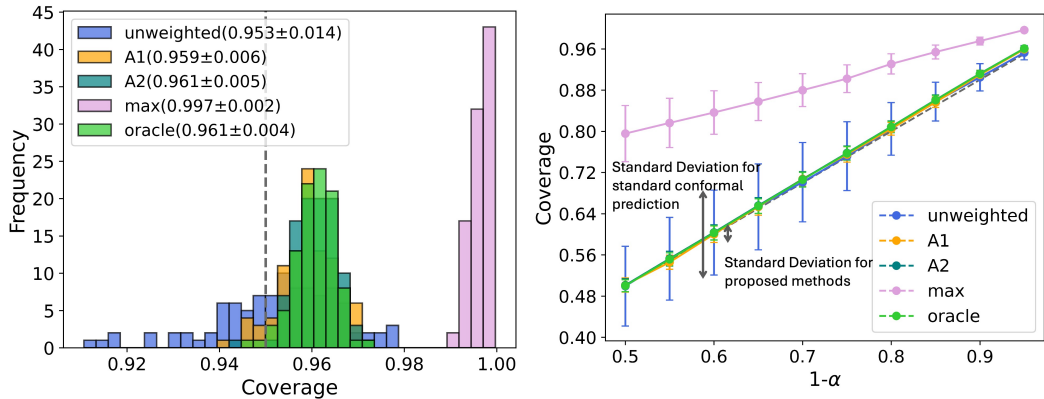


Figure 2: Coverage with 26 domains and 3 classes per domain. Vision transformer is calibrated with LAC score function for various algorithms. (Left) Coverage across 100 test environments at $\alpha = 0.05$. Each coverage data is the average of 15 calibration/test splits. Mean and standard deviations are shown in the legend. (Right) Mean and standard deviation of coverage across 100 test environments. Our algorithms (A1, A2, and oracle) demonstrate the desired coverage of 0.95 across test environments (unlike unweighted) and with minimal over-coverage (unlike max). Further, the practical algorithms A1 and A2 quite closely match the ideal oracle coverage.

5 Experiments

5.1 Experimental Setup for vision tasks

Dataset. For the vision tasks, we use the ImageNet Large Scale Visual Recognition Challenge dataset [27], which contains 1000 classes. We split the validation data in two, half as the calibration set and the other half as the test set. The split is done multiple times as the coverage guarantee of conformal prediction is over the randomness of the calibration set. To simulate subpopulation shifts, we adopt the BREEDS methodology [29]. The method creates a tree structure where the leaf nodes are the 1000 classes and the internal nodes are superclasses. We picked the nodes at level 3 as our domains and the descendants of each node are the classes in each domain. To create a balanced train environment, we keep the number of classes in each domain the same by removing domains with non-sufficient number of classes and removing some classes from domains with too many classes. We test on two different number of classes, one with 26 domains with 3 classes each and the other with 15 domains and 17 classes each. To simulate the different test environments, we follow the sampling strategy from [15] to draw λ from a Dirichlet distribution with parameter α' . The parameter α' controls the heterogeneity, i.e., as $\alpha' \rightarrow 0$, λ is 1 for one domain and 0 for all others. As $\alpha' \rightarrow \infty$, λ becomes uniform which reduces the problem to the no subpopulation shift case. Code is available at https://github.com/mrreganwang/Conformal_Subpop_Shifts

Models. We test on three different pretrained models: resnet50 pretrained on ImageNet [12], vision transformer pretrained on ImageNet21k and finetuned on ImageNet 2021 [30, 9, 33], and vision transformer pretrained on WIT-400M image-text pairs by OpenAI using CLIP embedding and finetuned on ImageNet-1k [24, 7, 9, 33]. For the domain classifiers, we modified the fully-connected layers of the three pre-trained models. The modified fully-connected layers now includes three dense layers with sizes 2048, 1024, and 512. The output layer is a softmax layer with output size of either 26 or 15.

Domain Classifier Training. For training, only the last 3 fully connected layers are updated. The training uses Adam [18] with cross entropy loss. After training, the domain classifiers are then calibrated using Multi-domain temperature scaling introduced in [35] to reduce calibration error.

5.2 Main Results

Coverage with varying test environments. We calibrated a pre-trained vision transformer with LAC score function and tested it on test set sampled from 100 different test environments. The test environment consists of 26 domains, with 3 classes in each domain while the λ was sampled from a Dirichlet distribution with parameter 0.1. Each coverage datapoint is averaged across 15 random calibration/test split. The results are plotted in Figure 2. From Figure 2 (Left) we observe that all three proposed algorithms were able to provide coverage for all test environments while standard conformal prediction could not for some test environments. For the max method, which conformalize the model using the worst case method mentioned in section 2.2, we see that marginal coverage is satisfied for all test environments, however, they are severely over-covered. We also observe that when compared to the standard conformal prediction, the standard deviations for the proposed algorithms are much smaller. This shows the adaptiveness of the proposed algorithms to maintain the desired coverage across test environments. From Figure 2 (Right), we see that the proposed algorithms are able to maintain coverage, while ensuring low standard deviations across different $1 - \alpha$.

Coverage under different settings We obtained the coverage results with varying score functions, model architectures, and degree of subpopulation shifts which we present in Appendix C. The coverage results are consistent across different settings.

6 Experiments without knowledge of domains

We test our proposed Algorithm 3 with the same settings as Section 5. For the vision tasks, although the same calibration set is used, we do not assume knowledge of the domain label.

6.1 Experimental Setup for language tasks

Datasets To simulate different domains in generative language tasks, we use two distinct datasets: TriviaQA [16], a closed-book question answering dataset, and GSM8K [8], a mathematical reasoning benchmark. Specifically, we use 2,500 samples from the test split of TriviaQA and the full GSM8K test set, which contains 1,319 questions. To create the calibration and test data, we first randomly select 500 TriviaQA samples and 500 GSM8K samples to create the test set. The rest of the samples are used as the calibration set. To keep the calibration set balanced, we randomly removed 1181 TriviaQA samples, resulting in a calibration set with 1638 samples. We repeat this process 10 times. To simulate each test environment, we again draw λ from a dirichlet distribution with parameter 0.1 and remove test data from each of the two domains to match the λ .

Models We use LLaMA-3-8B [1] as the generative model and obtain responses via greedy decoding. Following prior work [19, 5], we employ GPT-4o [22] as the correctness evaluator, using the query, generated response, and ground truth answer(s) as input. To assess the similarity between test samples and calibration data points, we use the all-mpnet-base-v2 model from SentenceTransformers [25].

6.2 Results for vision tasks

Coverage with varying test environments. We obtain the results for Algorithm 3 with the same setup as section 5.2 and the results are plotted in Figure 3. From Figure 3 (Left) we observe that

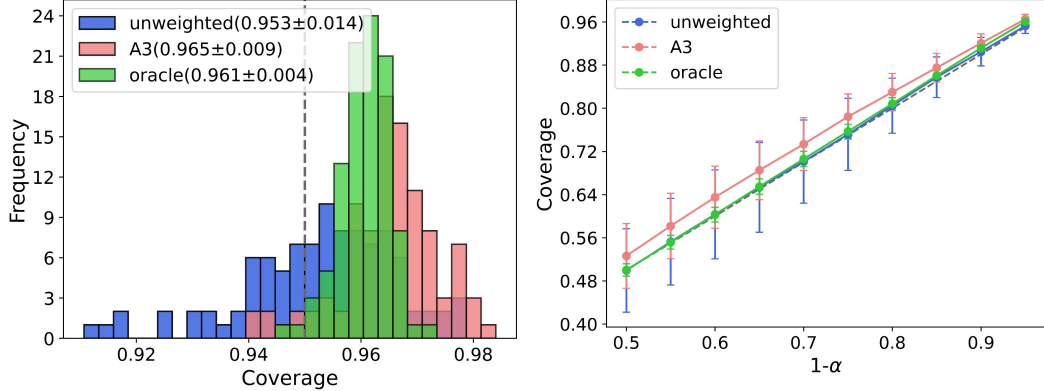


Figure 3: Coverage with 26 domains and 3 classes per domain. Vision transformer is calibrated with LAC score function for various algorithms. For the results of Algorithm 3, the parameters σ and β are 0.7 and 0.1 respectively. (Left) Coverage across 100 test environments at $\alpha = 0.05$. Each coverage data is the average of 15 calibration/test splits. Mean and standard deviations are shown in the legend. (Right) Mean and standard deviation of coverage across 100 test environments. Our algorithm (A3 in pink) demonstrates the desired coverage of 0.95 across test environments with minimal over-coverage. Further, even without using any distributional or domain information, it matches the ideal coverage of the oracle (in green) which knows the test distribution exactly.

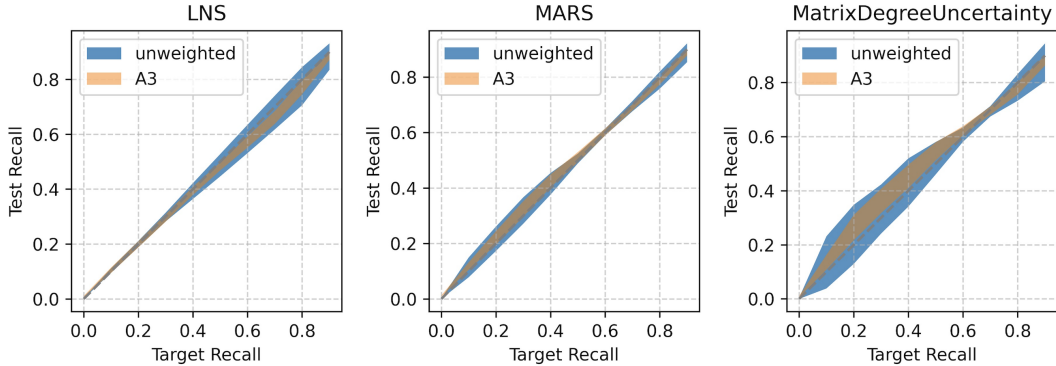


Figure 4: Distribution of test recall. LLaMA-3-8B was calibrated with 3 different score functions and test data were labeled according to 4.2. Recall was calculated with the standard deviation plotted. The standard deviation is across 100 different test environments, obtained by sampling Dirichlet distribution with $\alpha' = 0.5$. Standard LLM uncertainty estimation method (blue) is sensitive to distribution shifts as evidenced by the high variance in recall across test-environments, while the recall with our method A3 (orange) tightly follows the desired target recall.

Algorithm 3 was able to provide coverage for the majority of test environments while standard conformal prediction could not for a significant number of test environments. Although not as small as Algorithm 1 and 2, Algorithm 3 is still able to obtain smaller standard deviation than the standard conformal prediction which shows the adaptiveness of Algorithm 3 even without any knowledge of the domains. From Figure 3 (Right), we see that Algorithm 3 is able to maintain coverage, while ensuring low standard deviations across different $1 - \alpha$.

6.3 Results for language task

We obtain the results for algorithm described in 4.2 and shown in Figure 4. We see that the test recalls follow roughly to the target recall for both standard conformal prediction and the proposed Algorithm 3. However, standard conformal prediction produce results that have larger standard deviation than Algorithm 3. The results show the necessity of our algorithm for reliable decisions in the hallucination detection task in LLMs under various subpopulation shifts.

7 Conclusion, Limitations, and Future Work

This paper introduced three algorithms that extended conformal prediction to a setting with subpopulation shifts. For Algorithm 1, we proved that it provides a statistical guarantee to marginal coverage under the assumption that the domain classifier in the algorithm is multicalibrated. Similarly, for algorithm 2, we proved that it provides marginal coverage under the assumption that the domain classifier is multiaccurate. We evaluated the algorithms experimentally with a synthetic dataset which showed improvement from the standard conformal prediction algorithm in terms of providing coverage when standard conformal prediction did not.

A theoretical limitation of our method is that it does not take advantage of independence between samples from multiple domains which contributes to some over-coverage. This matters when the distribution shift is very mild, as we explore in the Appendix. Improving this is one interesting future work direction. On the practical side, our results do not provide guidance on what score function to pick. Also, our current work explores a single objective - generalizing conformal risk control in LLMs to reliably simultaneously control multiple risks such as hallucination, toxicity, sychophany, etc. is a practically impactful future direction.

8 Broader Impact

As people become increasingly dependent on AI models, uncertainty quantification for these models are ever more crucial. In most real-world settings, distribution shifts are almost impossible to avoid which necessitates uncertainty quantification methods that are adaptive to remedy the impacts. Our work examines the setting of test time distribution shifts which has a broad range of applications in deploying safe and trustworthy AI models.

Acknowledgments and Disclosure of Funding

YB and SPK were partially funded by Captil One CREDIF fellowship and grant respectively. SPK also thanks Yaodong Yu for initial conversations on this research.

References

- [1] AI@Meta. Llama 3 model card. 2024.
- [2] Anastasios Angelopoulos, Stephen Bates, Jitendra Malik, and Michael I. Jordan. Uncertainty sets for image classifiers using conformal prediction, 2022.
- [3] Anastasios N. Angelopoulos and Stephen Bates. A gentle introduction to conformal prediction and distribution-free uncertainty quantification. *CoRR*, abs/2107.07511, 2021.
- [4] Anastasios N. Angelopoulos, Stephen Bates, Adam Fisch, Lihua Lei, and Tal Schuster. Conformal risk control, 2023.
- [5] Yavuz Faruk Bakman, Duygu Nur Yaldiz, Baturalp Buyukates, Chenyang Tao, Dimitrios Dimitriadis, and Salman Avestimehr. MARS: Meaning-aware response scoring for uncertainty estimation in generative LLMs. In Lun-Wei Ku, Andre Martins, and Vivek Srikumar, editors, *Proceedings of the 62nd Annual Meeting of the Association for Computational Linguistics (Volume 1: Long Papers)*, pages 7752–7767, Bangkok, Thailand, August 2024. Association for Computational Linguistics.
- [6] Maxime Cauchois, Suyash Gupta, Alnur Ali, and John C. Duchi. Robust validation: Confident predictions even when distributions shift. *Journal of the American Statistical Association*, 119(548):3033–3044, February 2024.
- [7] Mehdi Cherti, Romain Beaumont, Ross Wightman, Mitchell Wortsman, Gabriel Ilharco, Cade Gordon, Christoph Schuhmann, Ludwig Schmidt, and Jenia Jitsev. Reproducible scaling laws for contrastive language-image learning. *arXiv preprint arXiv:2212.07143*, 2022.

- [8] Karl Cobbe, Vineet Kosaraju, Mohammad Bavarian, Mark Chen, Heewoo Jun, Lukasz Kaiser, Matthias Plappert, Jerry Tworek, Jacob Hilton, Reiichiro Nakano, Christopher Hesse, and John Schulman. Training verifiers to solve math word problems. *arXiv preprint arXiv:2110.14168*, 2021.
- [9] Alexey Dosovitskiy, Lucas Beyer, Alexander Kolesnikov, Dirk Weissenborn, Xiaohua Zhai, Thomas Unterthiner, Mostafa Dehghani, Matthias Minderer, Georg Heigold, Sylvain Gelly, Jakob Uszkoreit, and Neil Houlsby. An image is worth 16x16 words: Transformers for image recognition at scale. *ICLR*, 2021.
- [10] Parikshit Gopalan, Michael P. Kim, Mihir Singhal, and Shengjia Zhao. Low-degree multicalibration, 2022.
- [11] Dutch Hansen, Siddartha Devic, Preetum Nakkiran, and Vatsal Sharan. When is multicalibration post-processing necessary?, 2024.
- [12] Kaiming He, Xiangyu Zhang, Shaoqing Ren, and Jian Sun. Deep residual learning for image recognition, 2015.
- [13] Pengcheng He, Xiaodong Liu, Jianfeng Gao, and Weizhu Chen. Deberta: Decoding-enhanced bert with disentangled attention. In *International Conference on Learning Representations*, 2021.
- [14] Úrsula Hébert-Johnson, Michael P. Kim, Omer Reingold, and Guy N. Rothblum. Calibration for the (computationally-identifiable) masses. *CoRR*, abs/1711.08513, 2017.
- [15] Tzu-Ming Harry Hsu, Hang Qi, and Matthew Brown. Measuring the effects of non-identical data distribution for federated visual classification, 2019.
- [16] Mandar Joshi, Eunsol Choi, Daniel Weld, and Luke Zettlemoyer. TriviaQA: A large scale distantly supervised challenge dataset for reading comprehension. In Regina Barzilay and Min-Yen Kan, editors, *Proceedings of the 55th Annual Meeting of the Association for Computational Linguistics (Volume 1: Long Papers)*, pages 1601–1611, Vancouver, Canada, July 2017. Association for Computational Linguistics.
- [17] Michael P. Kim, Amirata Ghorbani, and James Y. Zou. Multiaccuracy: Black-box post-processing for fairness in classification. *CoRR*, abs/1805.12317, 2018.
- [18] Diederik P. Kingma and Jimmy Ba. Adam: A method for stochastic optimization, 2017.
- [19] Zhen Lin, Shubhendu Trivedi, and Jimeng Sun. Generating with confidence: Uncertainty quantification for black-box large language models. *Transactions on Machine Learning Research*, 2024.
- [20] Charles Lu, Yaodong Yu, Sai Praneeth Karimireddy, Michael I. Jordan, and Ramesh Raskar. Federated conformal predictors for distributed uncertainty quantification, 2023.
- [21] Andrey Malinin and Mark Gales. Uncertainty estimation in autoregressive structured prediction. In *International Conference on Learning Representations*, 2021.
- [22] OpenAI. GPT-4 Technical Report, 2023.
- [23] Drew Prinster, Samuel Stanton, Anqi Liu, and Suchi Saria. Conformal validity guarantees exist for any data distribution (and how to find them), 2024.
- [24] Alec Radford, Jong Wook Kim, Chris Hallacy, A. Ramesh, Gabriel Goh, Sandhini Agarwal, Girish Sastry, Amanda Askell, Pamela Mishkin, Jack Clark, Gretchen Krueger, and Ilya Sutskever. Learning transferable visual models from natural language supervision. In *ICML*, 2021.
- [25] Nils Reimers and Iryna Gurevych. Sentence-bert: Sentence embeddings using siamese bert networks. In *Proceedings of the 2019 Conference on Empirical Methods in Natural Language Processing*. Association for Computational Linguistics, 11 2019.

- [26] Yaniv Romano, Matteo Sesia, and Emmanuel J. Candès. Classification with valid and adaptive coverage, 2020.
- [27] Olga Russakovsky, Jia Deng, Hao Su, Jonathan Krause, Sanjeev Satheesh, Sean Ma, Zhiheng Huang, Andrej Karpathy, Aditya Khosla, Michael Bernstein, Alexander C. Berg, and Li Fei-Fei. ImageNet Large Scale Visual Recognition Challenge. *International Journal of Computer Vision (IJCV)*, 115(3):211–252, 2015.
- [28] Mauricio Sadinle, Jing Lei, and Larry Wasserman. Least ambiguous set-valued classifiers with bounded error levels. *Journal of the American Statistical Association*, 114(525):223–234, June 2018.
- [29] Shibani Santurkar, Dimitris Tsipras, and Aleksander Madry. Breeds: Benchmarks for subpopulation shift, 2020.
- [30] Andreas Steiner, Alexander Kolesnikov, , Xiaohua Zhai, Ross Wightman, Jakob Uszkoreit, and Lucas Beyer. How to train your vit? data, augmentation, and regularization in vision transformers. *arXiv preprint arXiv:2106.10270*, 2021.
- [31] Ryan J. Tibshirani, Rina Foygel Barber, Emmanuel J. Candes, and Aaditya Ramdas. Conformal prediction under covariate shift, 2020.
- [32] Vladimir Vovk, Alex Gammerman, and Glenn Shafer. *Algorithmic Learning in a Random World*. Springer-Verlag, Berlin, Heidelberg, 2005.
- [33] Ross Wightman. Pytorch image models. <https://github.com/huggingface/pytorch-image-models>, 2019.
- [34] Yuzhe Yang, Haoran Zhang, Dina Katabi, and Marzyeh Ghassemi. Change is hard: A closer look at subpopulation shift, 2023.
- [35] Yaodong Yu, Stephen Bates, Yi Ma, and Michael I. Jordan. Robust calibration with multi-domain temperature scaling, 2022.

A Proofs

A.1 Proof of Theorem 3.1

This proof follows the proof for Theorem 4.3 from [20] with some modifications. Suppose \mathcal{E} is the event

$$\mathcal{E} = \{\forall k \in [K], \exists \pi_k, (S_{\pi_k(1)}^k, \dots, S_{\pi_k(n_k)}^k, S_{\pi_k(n_k+1)}^k) = (s_1^k, \dots, s_{n_k}^k, s_{n_k+1}^k)\},$$

where $\{s_i^k\}_{i \in [n_k+1], k \in [K]}$ is the sorted numerical values of the score values. Furthermore, suppose c is a perfect classifier, i.e., $c(X) = c^*(X)$ for all $X \in \mathcal{X}$ where c^* is the true predictor in predicting λ . Therefore, we have that

$$\begin{aligned} Pr(S(X_{\text{test}}, Y_{\text{test}}; \hat{f}) \leq \hat{q}_\alpha | \mathcal{E}) \\ = \sum_{k=1}^K \lambda_k Pr(S(X_{\text{test}}, Y_{\text{test}}; \hat{f}) \leq \hat{q}_\alpha | \{S(X_1^k, Y_1^k; \hat{f}), \dots, \\ S(X_{n_k}^k, Y_{n_k}^k; \hat{f}), S(X_{\text{test}}, Y_{\text{test}}; \hat{f})\} \text{ are exchangeable}, \mathcal{E}). \end{aligned}$$

Since $S(X_1^k, Y_1^k; \hat{f}), \dots, S(X_{n_k}^k, Y_{n_k}^k; \hat{f}), S(X_{\text{test}}, Y_{\text{test}}; \hat{f})$ are exchangeable, we have that the above expression is lower bounded by

$$\sum_{k=1}^K \frac{\lambda_k m_k(\hat{q}_\alpha)}{n_k + 1},$$

which is lower bounded by $1 - \alpha$ by definition of \hat{q}_α . Therefore, we have that

$$Pr(S(X_{\text{test}}, Y_{\text{test}}; \hat{f}) \leq \hat{q}_\alpha | \mathcal{E}) \geq 1 - \alpha.$$

Since this holds for every $(s_1^k, \dots, s_{n_k}^k, s_{n_k+1}^k)$ for all $k \in [K]$, taking the expectation on both sides gives us

$$Pr(S(X_{\text{test}}, Y_{\text{test}}; \hat{f}) \leq \hat{q}_\alpha) \geq 1 - \alpha,$$

which completes the proof.

A.2 Proof of Theorem 3.3

This proof follows the proof for Theorem 4.3 from [20] with some modifications. Suppose \mathcal{E} is the event

$$\mathcal{E} = \{\forall k \in [K], \exists \pi_k, (S_{\pi_k(1)}^k, \dots, S_{\pi_k(n_k)}^k, S_{\pi_k(n_k+1)}^k) = (s_1^k, \dots, s_{n_k}^k, s_{n_k+1}^k)\},$$

where $\{s_i^k\}_{i \in [n_k+1], k \in [K]}$ is the sorted numerical values of the score values. Furthermore, suppose c is multicalibrated with respect to \mathcal{G} , the set of all test environments. Therefore, conditioned on \mathbb{P}_{test} , and $c(X_{\text{test}}) = \hat{\lambda}$, we have that $\mathbb{E}(c^*(X_{\text{test}}) | c(X_{\text{test}}) = \hat{\lambda}, (X_{\text{test}}, Y_{\text{test}}) \sim \mathbb{P}_{\text{test}}) = \hat{\lambda}$, where c^* is the true predictor in predicting λ . Combining this property with the partial exchangeable assumption, we have that

$$\begin{aligned} Pr(S(X_{\text{test}}, Y_{\text{test}}; \hat{f}) \leq \hat{q}_\alpha | (X_{\text{test}}, Y_{\text{test}}) \sim \mathbb{P}_{\text{test}}, c(X_{\text{test}}) = \hat{\lambda}, \mathcal{E}) \\ = \sum_{k=1}^K \hat{\lambda}_k Pr(S(X_{\text{test}}, Y_{\text{test}}; \hat{f}) \leq \hat{q}_\alpha | \{S(X_1^k, Y_1^k; \hat{f}), \dots, \\ S(X_{n_k}^k, Y_{n_k}^k; \hat{f}), S(X_{\text{test}}, Y_{\text{test}}; \hat{f})\} \text{ are exchangeable}, \mathcal{E}). \end{aligned}$$

Since $S(X_1^k, Y_1^k; \hat{f}), \dots, S(X_{n_k}^k, Y_{n_k}^k; \hat{f}), S(X_{\text{test}}, Y_{\text{test}}; \hat{f})$ are exchangeable, we have that the above expression is lower bounded by

$$\sum_{k=1}^K \frac{\hat{\lambda}_k m_k(\hat{q}_\alpha)}{n_k + 1},$$

which is lower bounded by $1 - \alpha$ by definition of \hat{q}_α . Therefore, we have that

$$Pr(S(X_{\text{test}}, Y_{\text{test}}; \hat{f}) \leq \hat{q}_\alpha | (X_{\text{test}}, Y_{\text{test}}) \sim \mathbb{P}_{\text{test}}, c(X_{\text{test}}) = \hat{\lambda}, \mathcal{E}) \geq 1 - \alpha.$$

Since this holds for every $(s_1^k, \dots, s_{n_k}^k, s_{n_k+1}^k)$ for all $k \in [K]$, taking the expectation on both sides gives us

$$Pr(S(X_{\text{test}}, Y_{\text{test}}; \hat{f}) \leq \hat{q}_\alpha | (X_{\text{test}}, Y_{\text{test}}) \sim \mathbb{P}_{\text{test}}, c(X_{\text{test}}) = \hat{\lambda}) \geq 1 - \alpha.$$

Finally, by law of total probability over all possible $c(X_{\text{test}})$ we get that

$$Pr(S(X_{\text{test}}, Y_{\text{test}}; \hat{f}) \leq \hat{q}_\alpha | (X_{\text{test}}, Y_{\text{test}}) \sim \mathbb{P}_{\text{test}}) \geq 1 - \alpha,$$

which completes the proof.

A.3 Proof of Theorem 3.5

This proof follows the proof for Theorem 4.3 from [20] with some modifications. Suppose \mathcal{E} is the event

$$\mathcal{E} = \{\forall k \in [K], \exists \pi_k, (S_{\pi_k(1)}^k, \dots, S_{\pi_k(n_k)}^k, S_{\pi_k(n_k+1)}^k) = (s_1^k, \dots, s_{n_k}^k, s_{n_k+1}^k)\},$$

where $\{s_i^k\}_{i \in [n_k+1], k \in [K]}$ is the sorted numerical values of the score values. Furthermore, suppose c is multiaccurate with respect to \mathcal{G} , the set of all test environments. Therefore, conditioned on \mathbb{P}_{test} , we have that $\mathbb{E}(c^*(X_{\text{test}}) | (X_{\text{test}}, Y_{\text{test}}) \sim \mathbb{P}_{\text{test}}) = \mathbb{E}(\hat{\lambda} | (X_{\text{test}}, Y_{\text{test}}) \sim \mathbb{P}_{\text{test}})$, where c^* is the true predictor in predicting λ and $\hat{\lambda} = c(X_{\text{test}})$. Combining this property with the partial exchangeable assumption, we have that

$$\begin{aligned} Pr(S(X_{\text{test}}, Y_{\text{test}}; \hat{f}) \leq \hat{q}_\alpha | (X_{\text{test}}, Y_{\text{test}}) \sim \mathbb{P}_{\text{test}}, \mathcal{E}) \\ = \sum_{k=1}^K \hat{\lambda}_k Pr(S(X_{\text{test}}, Y_{\text{test}}; \hat{f}) \leq \hat{q}_\alpha | \{S(X_1^k, Y_1^k; \hat{f}), \dots, \\ S(X_{n_k}^k, Y_{n_k}^k; \hat{f}), S(X_{\text{test}}, Y_{\text{test}}; \hat{f})\} \text{ are exchangeable}, \mathcal{E}). \end{aligned}$$

Since $S(X_1^k, Y_1^k; \hat{f}), \dots, S(X_{n_k}^k, Y_{n_k}^k; \hat{f}), S(X_{\text{test}}, Y_{\text{test}}; \hat{f})$ are exchangeable, we have that the above expression is lower bounded by

$$\sum_{k=1}^K \frac{\hat{\lambda}_k m_k(\hat{q}_\alpha)}{n_k + 1},$$

which is lower bounded by $1 - \alpha$ by definition of \hat{q}_α . Therefore, we have that

$$Pr(S(X_{\text{test}}, Y_{\text{test}}; \hat{f}) \leq \hat{q}_\alpha | (X_{\text{test}}, Y_{\text{test}}) \sim \mathbb{P}_{\text{test}}, \mathcal{E}) \geq 1 - \alpha.$$

Since this holds for every $(s_1^k, \dots, s_{n_k}^k, s_{n_k+1}^k)$ for all $k \in [K]$, taking the expectation on both sides gives us

$$Pr(S(X_{\text{test}}, Y_{\text{test}}; \hat{f}) \leq \hat{q}_\alpha | (X_{\text{test}}, Y_{\text{test}}) \sim \mathbb{P}_{\text{test}}) \geq 1 - \alpha,$$

which completes the proof.

B Overview of Score Functions

Although conformal prediction algorithms provide marginal coverage guarantees for arbitrary score functions, a poorly designed score function can lead to uninformative prediction sets. For our experiments we explore 3 different score functions for both vision and language tasks.

B.1 Vision Tasks

We explore the following commonly used score functions for the vision tasks:

- Least Ambiguous Set-valued Classifier (*LAC*) [28]. Given data (X, y) where y is the true label of X , define $S(X, y; \hat{f})$ as

$$S(X, y; \hat{f}) = 1 - f(X)_y.$$

- Adaptive Prediction Set (*APS*) [26]. Given data (X, y) where y is the true label of X , define $S(X, y; \hat{f})$ as

$$S(X, y; \hat{f}) = \sum_{i=1}^k f(X)_{\pi(i)},$$

where π sorts the labels in descending order of label probability given by $f(X)$ and $k = \pi(y)$. In other words, we add up the label probabilities in descending order until we added the true label probability.

- Regularized Adaptive Prediction Set (*RAPS*) [2]. Given data (X, y) where y is the true label of X , define $S(X, y; \hat{f})$ as

$$S(X, y; \hat{f}) = \left(\sum_{i=1}^k f(X)_{\pi(i)} \right) + a * \max(k - b, 0),$$

where π sorts the labels in descending order of label probability given by $f(X)$, $k = \pi(y)$, and (a, b) are regularization parameters.

B.2 Language Tasks

We explore the following commonly used score functions for the language tasks:

- Length Normalized Scoring (*LNS*) [21]. Given a query X and the generated response $\mathbf{y} = \{y_1, y_2, \dots, y_L\}$ of length L , define $S(X, \mathbf{y}; \hat{f})$ as the average log probability of the generated sequence, i.e.,

$$S(X, \mathbf{y}) = \frac{1}{L} \sum_{i=1}^L \log \Pr[y_i | y_{<i}, X; \hat{f}],$$

where y_i represents the i -th token in the sequence and $y_{<i}$ represents the tokens generated before y_i .

- Meaning-Aware Response Scoring (*MARS*) [5]. Given a query X and the generated response $\mathbf{y} = \{y_1, y_2, \dots, y_L\}$ of length L , define $S(X, \mathbf{y}; \hat{f})$ as

$$S(X, \mathbf{y}; \hat{f}) = \prod_{i=1}^L \Pr[y_i | y_{<i}, X; \hat{f}]^{w(\mathbf{y}, X, L, i)},$$

where w represents the token weight that emphasize tokens that contribute to answering the query.

- Degree Matrix Uncertainty [19]. We adopt the uncertainty estimate definition of [19] where the score only depends on the query X . Given a query X and m generated responses $\mathbf{y}_1, \mathbf{y}_2, \dots, \mathbf{y}_m$, first, define W as a matrix of pairwise entailment dependencies where W_{ij} represents the entailment dependency between output response \mathbf{y}_i and \mathbf{y}_j . Entailment dependencies are calculated by using a Natural Language Inference classifier [13] that classifies generated responses into three classes: entailment, neutral, or contradiction. We then define the degree matrix D as

$$D_{ii} = \sum_{j=1}^m W_{ij}.$$

Lastly, the score is defined as

$$\frac{\text{trace}(mI - D)}{m^2}.$$

C Additional Experiments on Adapting to Distribution Shifts with Domain Knowledge

Table 1: Coverage at $\alpha = 0.1$ with 26 domains and 3 classes per domain. The results vary over 3 architectures (VisionTransfomer, Resnet50, and Clip) and 3 score functions (*LAC*, *APS*, and *RAPS*). The mean and standard deviation across 100 test environments, sampled from Dirichlet distribution with $\alpha' = 0.1$, are recorded. For each of the 100 test environments, coverage result is averaged over 15 random calibration/test splits. The results show that the proposed algorithms consistently outperform standard conformal prediction by having lower standard deviations across the 100 test environments.

		unweighted	oracle	A1	A2
ViT	<i>LAC</i>	0.905 ± 0.026	0.912 ± 0.006	0.910 ± 0.009	0.912 ± 0.006
	<i>APS</i>	0.904 ± 0.021	0.912 ± 0.005	0.909 ± 0.006	0.912 ± 0.005
	<i>RAPS</i>	0.903 ± 0.016	0.910 ± 0.008	0.909 ± 0.008	0.911 ± 0.007
Resnet50	<i>LAC</i>	0.907 ± 0.027	0.911 ± 0.008	0.909 ± 0.009	0.912 ± 0.008
	<i>APS</i>	0.905 ± 0.022	0.910 ± 0.007	0.907 ± 0.007	0.911 ± 0.007
	<i>RAPS</i>	0.903 ± 0.015	0.908 ± 0.008	0.904 ± 0.009	0.909 ± 0.007
Clip	<i>LAC</i>	0.909 ± 0.023	0.912 ± 0.007	0.910 ± 0.007	0.912 ± 0.007
	<i>APS</i>	0.908 ± 0.021	0.913 ± 0.008	0.910 ± 0.007	0.914 ± 0.008
	<i>RAPS</i>	0.902 ± 0.014	0.910 ± 0.005	0.909 ± 0.006	0.910 ± 0.005

Table 2: Coverage at $\alpha = 0.1$ with 26 domains and 3 classes per domain. The results vary over 3 architectures (VisionTransfomer, Resnet50, and Clip) and 3 score functions (*LAC*, *APS*, and *RAPS*). The mean and standard deviation across 100 test environments, sampled from Dirichlet distribution with $\alpha' = 1$, are recorded. For each of the 100 test environments, coverage result is averaged over 15 random calibration/test splits. The results show that the proposed algorithms consistently outperform standard conformal prediction by having lower standard deviations across the 100 test environments. The results also show that the difference between standard deviations of standard and the proposed methods are much smaller than those from Table 1. This is a limitation to our proposed algorithms which do not assume independence between data from different domains, leading to more conservative bounds for coverage in this case where the subpopulation shifts are milder (larger α').

		unweighted	oracle	A1	A2
ViT	<i>LAC</i>	0.899 ± 0.011	0.912 ± 0.003	0.910 ± 0.004	0.912 ± 0.003
	<i>APS</i>	0.900 ± 0.007	0.912 ± 0.003	0.908 ± 0.003	0.912 ± 0.003
	<i>RAPS</i>	0.900 ± 0.007	0.912 ± 0.004	0.908 ± 0.003	0.912 ± 0.003
Resnet50	<i>LAC</i>	0.899 ± 0.011	0.912 ± 0.003	0.907 ± 0.004	0.913 ± 0.003
	<i>APS</i>	0.902 ± 0.008	0.913 ± 0.003	0.908 ± 0.004	0.914 ± 0.003
	<i>RAPS</i>	0.898 ± 0.006	0.911 ± 0.004	0.905 ± 0.003	0.911 ± 0.003
Clip	<i>LAC</i>	0.901 ± 0.010	0.913 ± 0.003	0.910 ± 0.003	0.913 ± 0.003
	<i>APS</i>	0.904 ± 0.008	0.916 ± 0.004	0.910 ± 0.003	0.916 ± 0.003
	<i>RAPS</i>	0.900 ± 0.005	0.911 ± 0.003	0.908 ± 0.003	0.911 ± 0.003

Table 3: Coverage at $\alpha = 0.1$ with 15 domains and 17 classes per domain. The results vary over 3 architectures (VisionTransformer, Resnet50, and Clip) and 3 score functions (*LAC*, *APS*, and *RAPS*). The mean and standard deviation across 100 test environments, sampled from Dirichlet distribution with $\alpha' = 0.1$, are recorded. For each of the 100 test environments, coverage result is averaged over 15 random calibration/test splits. The results show that the proposed algorithms consistently outperform standard conformal prediction by having lower standard deviations across the 100 test environments. Compared to the results from Table 1, the standard deviations are lower across all algorithms and the mean is much closer to the desired 0.9. The larger number of calibration data here results in a tighter coverage distribution due to the randomness of marginal coverage guarantee for conformal prediction algorithms.

		unweighted	oracle	A1	A2
ViT	<i>LAC</i>	0.902 ± 0.024	0.901 ± 0.003	0.900 ± 0.005	0.901 ± 0.003
	<i>APS</i>	0.902 ± 0.015	0.905 ± 0.003	0.904 ± 0.003	0.904 ± 0.003
	<i>RAPS</i>	0.901 ± 0.009	0.902 ± 0.003	0.902 ± 0.003	0.902 ± 0.003
Resnet50	<i>LAC</i>	0.901 ± 0.028	0.902 ± 0.004	0.901 ± 0.006	0.901 ± 0.005
	<i>APS</i>	0.900 ± 0.026	0.902 ± 0.004	0.901 ± 0.004	0.902 ± 0.004
	<i>RAPS</i>	0.900 ± 0.019	0.902 ± 0.003	0.901 ± 0.004	0.901 ± 0.004
Clip	<i>LAC</i>	0.902 ± 0.023	0.901 ± 0.004	0.901 ± 0.005	0.901 ± 0.004
	<i>APS</i>	0.900 ± 0.024	0.902 ± 0.003	0.901 ± 0.003	0.902 ± 0.003
	<i>RAPS</i>	0.901 ± 0.011	0.900 ± 0.003	0.900 ± 0.003	0.900 ± 0.003

Table 4: Coverage at $\alpha = 0.1$ with 15 domains and 7 classes per domain. The results vary over 3 architectures (VisionTransformer, Resnet50, and Clip) and 3 score functions (*LAC*, *APS*, and *RAPS*). The mean and standard deviation across 100 test environments, sampled from Dirichlet distribution with $\alpha' = 1$, are recorded. For each of the 100 test environments, coverage result is averaged over 15 random calibration/test splits. The results show that the proposed algorithms consistently outperform standard conformal prediction by having lower standard deviations across the 100 test environments. The results also show that the difference between standard deviations of standard and the proposed methods are much smaller than those from Table 3 due to the limitations of the proposed algorithms.

		unweighted	oracle	A1	A2
ViT	<i>LAC</i>	0.900 ± 0.009	0.901 ± 0.002	0.899 ± 0.002	0.901 ± 0.002
	<i>APS</i>	0.905 ± 0.006	0.905 ± 0.001	0.905 ± 0.001	0.905 ± 0.001
	<i>RAPS</i>	0.901 ± 0.003	0.903 ± 0.002	0.902 ± 0.002	0.903 ± 0.002
Resnet50	<i>LAC</i>	0.902 ± 0.010	0.902 ± 0.002	0.901 ± 0.002	0.902 ± 0.002
	<i>APS</i>	0.903 ± 0.010	0.903 ± 0.002	0.901 ± 0.002	0.903 ± 0.002
	<i>RAPS</i>	0.901 ± 0.007	0.902 ± 0.002	0.901 ± 0.002	0.902 ± 0.002
Clip	<i>LAC</i>	0.899 ± 0.009	0.901 ± 0.002	0.901 ± 0.002	0.901 ± 0.002
	<i>APS</i>	0.902 ± 0.008	0.902 ± 0.001	0.901 ± 0.001	0.902 ± 0.001
	<i>RAPS</i>	0.900 ± 0.004	0.902 ± 0.002	0.900 ± 0.002	0.901 ± 0.002

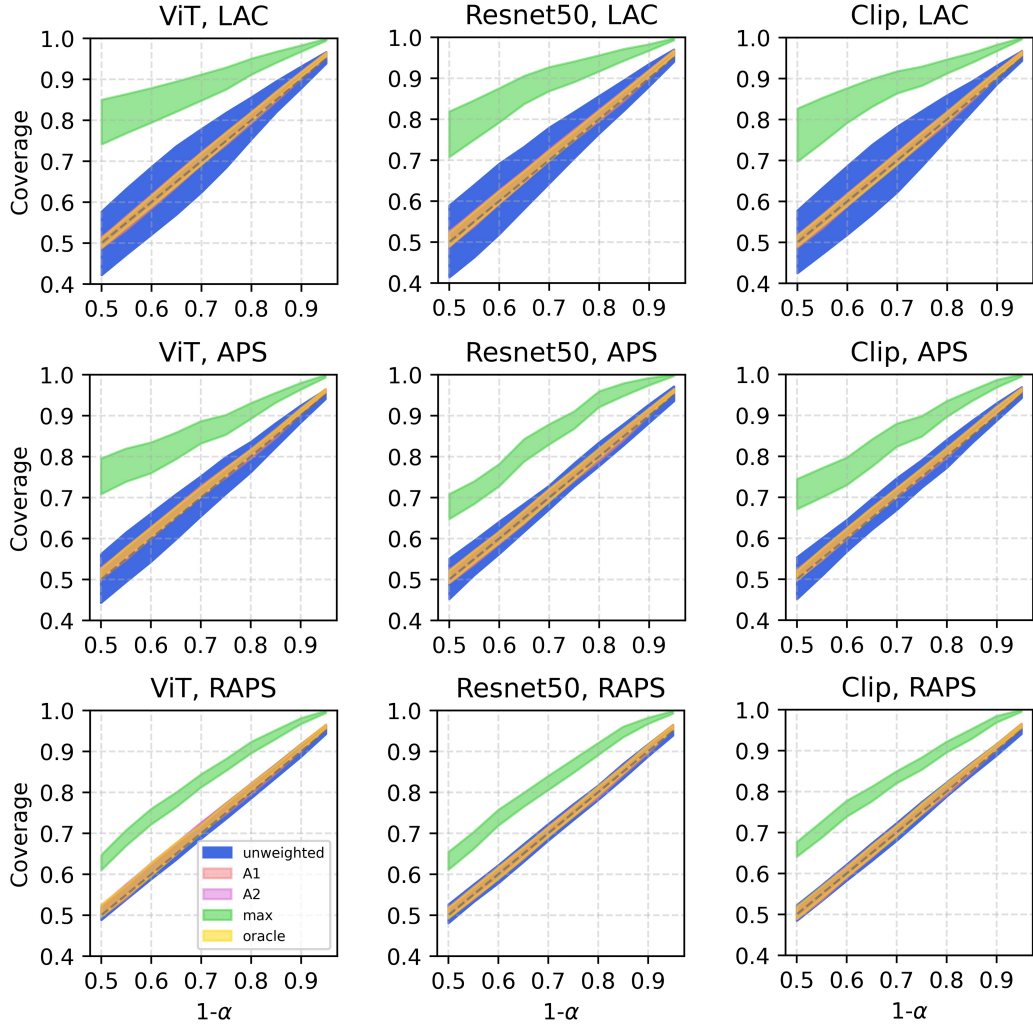


Figure 5: Distribution of coverage across different $1 - \alpha$. The results from 3 different model architectures (VisionTransformer, Resnet50, and Clip) and 3 different score functions (LAC, APS, and RAPS) are shown. For each sub-figure, the standard deviation across 100 test environments, sampled from Dirichlet distribution with $\alpha' = 0.1$, is plotted. For each test environment, the coverage result is the average of 15 random calibration/test splits. The domain structure consists of 26 domains and 3 classes per domain. The results show that the proposed algorithms consistently outperform standard conformal prediction by having lower standard deviations across all model architectures, score functions, and α .

D Additional Experiments on Adapting to Distribution Shifts without Domain Knowledge

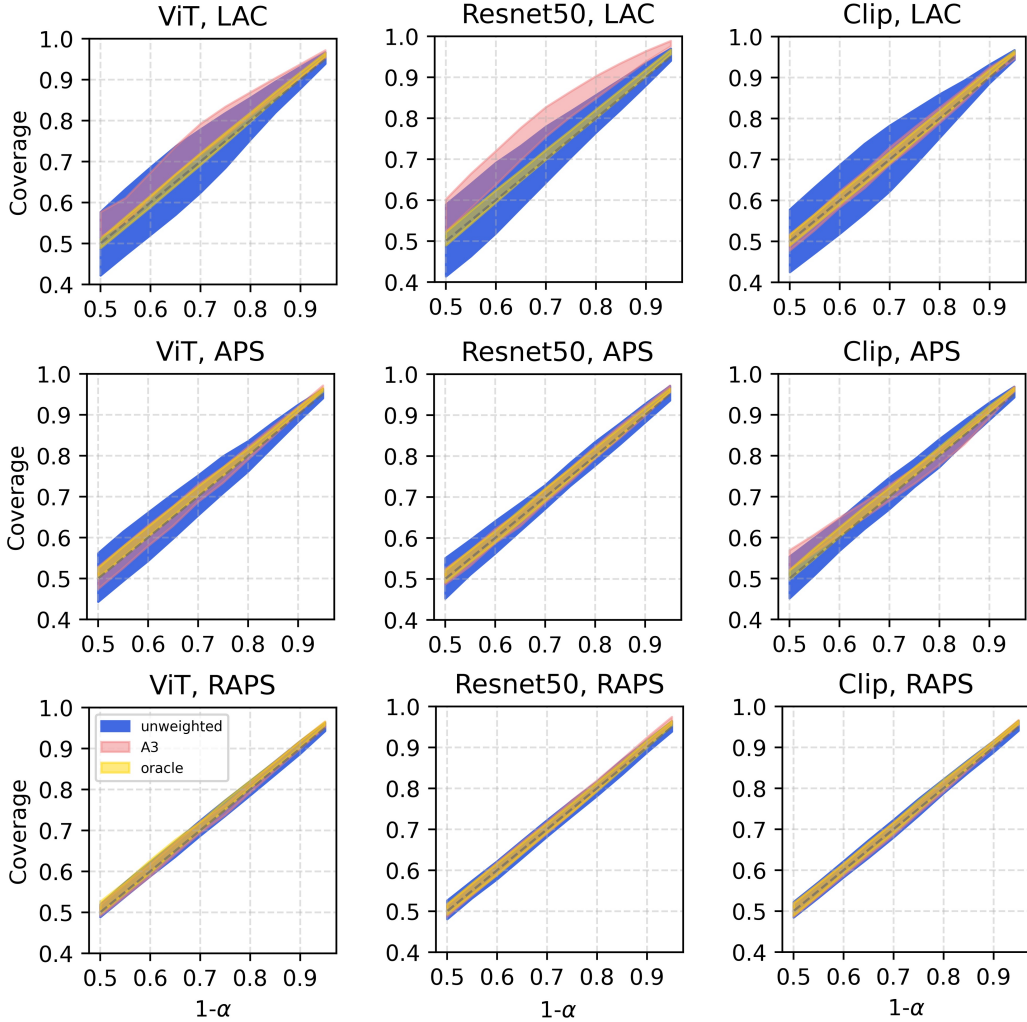


Figure 6: Distribution of coverage across different $1 - \alpha$ for Algorithm 3. For all settings, the top 5% of calibration data were selected and the temperature parameter σ was optimized for each α value as shown in Table 5. The results from 3 different model architectures (VisionTransformer, Resnet50, and Clip) and 3 different score functions (*LAC*, *APS*, and *RAPS*) are shown. For each sub-figure, the standard deviation across 100 test environments, sampled from Dirichlet distribution with $\alpha' = 0.1$, is plotted. For each test environment, the coverage result is the average of 15 random calibration/test splits. The domain structure consists of 26 domains and 3 classes per domain. The results show that the proposed algorithms consistently outperform standard conformal prediction by having lower standard deviations across all model architectures, score functions, and α . Smaller σ values show a lower standard deviation across the 100 test environments, however, it deviates the mean from the ideal $1 - \alpha$ coverage slightly. Conversely, larger σ results in larger standard deviation since Algorithm 3 reduces to the unweighted case as $\sigma \rightarrow \infty$. Therefore, choosing σ is a trade-off between mean and standard deviation across test environments.

Table 5: Parameter (σ) used to generate results from Figure 6

	α	0.05	0.1	0.15	0.2	0.25	0.3	0.35	0.4	0.45	0.5
ViT	<i>LAC</i>	2.05	1.65	1.30	1.00	0.75	0.55	0.40	0.30	0.25	0.20
	<i>APS</i>	0.70	0.70	0.70	0.70	0.70	0.55	0.55	0.50	0.50	0.45
	<i>RAPS</i>	1.00	0.70	0.70	0.70	0.70	0.50	0.50	0.50	0.45	0.45
Resnet50	<i>LAC</i>	0.70	0.70	0.70	0.70	0.70	0.70	0.70	0.70	0.70	0.70
	<i>APS</i>	1.50	1.50	1.00	0.70	0.60	0.50	0.50	0.40	0.40	0.35
	<i>RAPS</i>	2.00	2.00	1.50	1.50	1.00	0.80	0.70	0.70	0.70	0.70
Clip	<i>LAC</i>	2.00	0.55	0.45	0.36	0.30	0.26	0.24	0.22	0.21	0.20
	<i>APS</i>	0.70	0.70	0.70	0.70	0.70	0.70	0.70	0.70	0.70	0.70
	<i>RAPS</i>	0.70	0.70	0.70	0.70	0.70	0.70	0.70	0.70	0.70	0.70

E Compute Resources

An A40 GPU and 60GB of memory were used to compute all results or train the models. For the domain classifier, With a batch size of 32, the training took 15 hours for the 26 domain case and 48 hours for the 15 domain case.